Noname manuscript No.
(will be inserted by the editor)

Torsional oscillations of a sphere in a Stokes flow

F. Box · A. B. Thompson · T. Mullin

Received: date / Accepted: date

Abstract The results of an experimental investigation of a sphere performing torsional oscillations in a Stokes flow are presented. A novel experimental set up was developed which enabled the motion of the sphere to be remotely controlled through application of an oscillatory magnetic field. The response of the sphere to the applied field was characterised in terms of the viscous, magnetic and gravitational torques acting on the sphere. A mathematical model of the system was developed and good agreement was found between experimental, numerical and theoretical results. The flow resulting from the motion of the sphere was measured and the fluid velocity was found to have an inverse square dependence on radial distance from the sphere. The good agreement between measurements and the analytical solutions for both fluid velocity and angular displacement of the sphere indicates that the flow may be considered Stokesian, thus providing an excellent basis for experimental and theoretical characterisation of hydrodynamic interactions between multiple oscillating spheres at low Reynolds number.

Keywords torsional oscillations · sphere · Stokes flow · magnetic actuation

F. Box
Manchester Centre for Nonlinear Dynamics, School of Physics and Astronomy, University of Manchester, Oxford Road, Manchester, M13 9PL, UK
Present address: of F. Box
BP Institute for Multiphase Flow, Department for Earth Sciences, University of Cambridge, Madingley Road, Cambridge, CB3 0EZ, UK. Tel.: +44 1223-765700
E-mail: fb424@cam.ac.uk

A. B. Thompson
Manchester Centre for Nonlinear Dynamics, School of Mathematics, University of Manchester, Oxford Road, Manchester, M13 9PL, UK
Present address: of A. B. Thompson
Department of Mathematics, Imperial College London, London, SW7 2AZ, UK.

T. Mullin
Manchester Centre for Nonlinear Dynamics, School of Physics and Astronomy, University of Manchester, Oxford Road, Manchester, M13 9PL, UK

1 Introduction

The torsional oscillations of a sphere in a viscous fluid is a classical problem in fluid mechanics which has received significant theoretical study but relatively few experimental investigations since it was first considered in 1860 [11]. Moreover, the experimental work undertaken was performed on torsion pendulums - spheres supported in the fluid by a mechanically driven rod or torsion fibre - and did not consider the viscous effects introduced by the mechanical support [12, 10, 9, 2].

The effects of an inelastic tether on the motion of a particle in an oscillating flow have been shown, however, to be important at low frequencies of oscillation [20], while significant effects on viscous drag caused by fastening a string to a translating sphere have also been reported [6]. Whilst developing a 'spinning-ball viscometer' for measuring the rheological properties of suspensions, Mondy *et al.* [23] used the assumption that the total torque was a linear addition of the respective torques acting on the ball and the supporting rod and found comparable viscosities to independent measurements of Newtonian solvents performed with a conventional capillary viscometer⋆.

⋆ Mondy *et al.* [23] measured the couple experienced by a rotating ball immersed in a concentrated suspension of

We have developed a remote control approach to investigating the textbook [17] problem of a torsionally oscillating sphere, free of tethering, at low frequencies of oscillation and low Reynolds number, such that the Reynolds number based on the instantaneous fluid velocity $Re = av_{max}/\nu \ll 1$ (where a is the radius of the sphere, v_{max} is the maximum magnitude of fluid velocity and ν is the kinematic viscosity of the fluid). The frequency is parametrised by the Womersley parameter α where $\alpha^2 = a^2\omega/\nu$ (where ω is the angular frequency of the sphere) which is also much less than 1 here. For this choice of parameters the fluid velocity varies only slowly with time and can be regarded as steady at any given instant, such that the steady Stokes equations of fluid motion apply and the torque on the sphere can be considered to be quasi-steady [17].

In the classic monograph *Hydrodynamics*, Lamb [16] derived the analytic solution for a steadily rotating sphere, at $Re = 0$, and for a sphere performing small-amplitude torsional oscillations, at low but non-zero Re. In both cases, the sphere was assumed to be free and either in an infinite domain or rotating inside a larger concentric sphere. The fluid was shown to move around the oscillating sphere in concentric shells, centred on the axis of rotation. Similarly, for small-amplitude oscillations and negligible secondary fluid motion, the flow resulting from the decaying oscillations of a torsion pendulum was determined to be circumferential in annuli around the axis of rotation [4, 15].

Previous experimental investigations [10, 9, 2] have mainly focused on the damping of a torsion pendulum, and were performed for $Re > 1$. In the typical configuration, a sphere was suspended in the viscous fluid and deflected from the equilibrium position. A restoring couple acts on the supporting fibre such that the sphere approaches the equilibrium position through decaying oscillations. Folse [10] measured the gradual damping of a torsion pendulum and, in doing so, identified an algebraic error in the original calculation [5] of the correction term to the torque which, for $Re > 1$, results from the development of circulatory streaming motion [7]. Hollerbach *et al.* [12], in contrast, used a sphere supported from above and below by a mechanical rod which oscillated with a fixed period to examine the radial jet which results from colliding circulatory flows. Flow visualisation of the laminar to turbulent transition of the radial jet, that occurs for $Re = \mathcal{O}(200)^{\dagger}$, provided an explanation of the abrupt variation in the damping rate of the torsion pendulum found by Benson and Hollis Hallett [2] in experiments performed in liquid helium. The effect of the motion of the supporting fibre or rod present in both of these experimental investigations was not considered in the theoretical models where a free sphere was assumed. The authors are not aware of any experimental work conducted on a free sphere performing torsional oscillations, a fact which results from the inherent difficulty present in driving the motion of a body without mechanical contact.

Here, we present an investigation of the fluid motion induced by spheres which were forced to oscillate without mechanical contact in a Stokes flow. Near neutrally-buoyant spheres, with a magnetic dipole axis, were submerged in a very viscous fluid. Application of a steady magnetic field introduced a magnetic torque which acted to align the magnetic dipole of the sphere with the applied field causing the sphere to rotate. Through application of an alternating magnetic field, the sphere was made to perform torsional oscillations with an amplitude and a frequency determined by the magnitude and frequency of the applied field. The use of a magnetic field to control the translational motion of a sphere in a viscous fluid has been employed previously [1], but not, as far as the authors are aware, as a means of controlling the rotational motion of a sphere.

The experimental set up, which enabled characterisation of the response of a single sphere to magnetic actuation, is detailed in §2. The mathematical model of the sphere response to the applied field is described in §3. A comparison of the experimental and theoretical characterisation of the dynamic response of the sphere to magnetic actuation and measurements of the flow induced by the motion of the sphere are detailed in §4. The opportunities presented by the developed experimental system to investigate other hydrodynamic phenomena are discussed in §5

2 Experimental Set Up

A schematic diagram of the experimental set up used to characterise the dynamic response of the sphere to an applied magnetic field is shown in Figure 1a. Experiments were conducted on a polypropylene sphere of diameter $2a = 15.86 \pm 0.01$ mm (Dejay Distribution Ltd., UK). Two neodymium, permanent magnets were inserted into machined holes in the sphere and

comparatively-sized, neutrally buoyant spheres and compared it to the torque on a sphere spinning in a Newtonian fluid, uncovering an apparent slip which reduced the measured torque when the radius of the spinning ball becomes comparable with that of the suspended spheres.

† Hollerbach *et al.* define $Re = a\omega\delta/\nu$, where the penetration depth of the boundary layer $\delta = (2\nu/\omega)^{1/2}$, and provide an interesting discussion of the appropriate choice of Re [12].

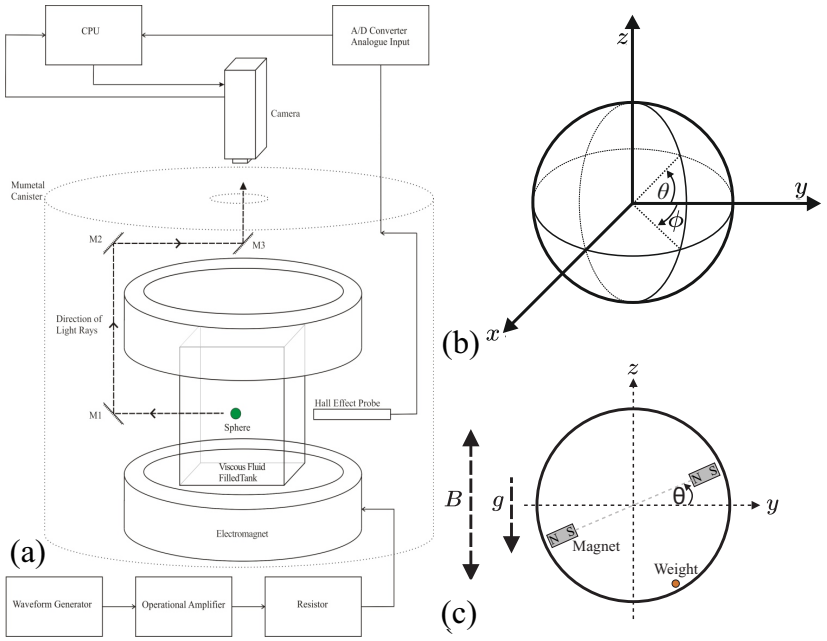

Fig. 1: (a) Schematic diagram of the experimental apparatus. Near neutrally-buoyant spheres in a viscous fluid filled tank were imaged using an optical arrangement of mirrors (M1, M2 and M3) and a computer-controlled camera. An unsteady magnetic field was applied using Helmholtz coils and measured by a Hall effect probe. The experimental system was contained within a Mumetal canister to reduce the effects of extraneous magnetic fields. (b) Schematic diagram of the coordinate system (*NB*: this definition θ is not common to all spherical polar coordinate systems), and (c) a projection of the coordinate system onto the observed plane for which $\phi = 0$. The projection of the coordinate system also includes indications of the direction of the applied magnetic field, B and the direction of gravity, g.

small amounts of glue were used to hold them in place. The two magnets were carefully embedded in the sphere such that they were flush with the surface and diametrically opposite ($\pm 1^\circ$) along an axis through the centre of the sphere. The permanent magnets were cylindrical, of length 3.00 ± 0.01 mm and diameter 2.48 ± 0.01 mm, occupying less than 2% of the sphere volume. The opposite poles of the magnets were placed facing one another such that the two magnets acted as a single dipole, the length of which was equal to the sphere diameter. The permanent magnets had a remanence of 1.19 ± 0.05 T and a coercivity ≥ 868 kA m^{-1} [27]. These values indicate that the strength of the magnets is large for their size compared to standard ferromagnetic materials which typically have a coercivity < 100 kA m^{-1}. The magnetic dipole moment of an individual magnet, $m = 0.0140 \pm 0.0006$ A m^2, was effectively independent of the applied magnetic field for the range of values used [13].

After the inclusion of the magnets, additional weights were embedded in the sphere in order to obtain near neutral buoyancy. The weights were austenitic stainless steel and non-magnetic. The sphere thus had a non-uniform mass distribution that introduced a gravitational torque towards a preferred orientation in the absence of applied magnetic field. The zero-field orientation of the magnetic dipole of the sphere was controlled by careful positioning of the embedded weights such that the magnetic dipole axis of the sphere was orientated approximately orthogonal to the applied field direction. The resulting density of the sphere was $\rho_s = 978.53 \pm 3.8$ kg m^{-3}.

The centre of mass was not at the centre of the sphere, but instead was displaced a small distance λa from the centre, and as such the magnetic dipole axis of the sphere resided at an angle θ_0 even when subjected to zero magnetic field. The calculation of λ (in the range 0 to 1) and θ_0 would require a complete knowledge of the density distribution within the sphere. Instead we use an experimental calibration based on the rate at which the sphere returns to $\theta = \theta_0$ if displaced from equilibrium in the absence of applied magnetic field, where θ is the angle between the magnetic dipole and the x-y plane, shown in the schematic diagram in Figure 1b. The time-scale associated with the gravitational torque acting on the sphere was measured, using the method outlined in §3.2, and found to be $T_0 = 4.67 \pm 0.03$ s. This calibration method is discussed further in §3.2, where

we conclude that $\theta_0 = 3.22 \pm 0.77°$ and $\lambda = 0.015$, so that the centre of mass is displaced very slightly from the centre of the sphere. However, the resulting gravitational moment due to the offset centre of mass still has a significant effect on the dynamics of the ball in response to the imposed magnetic field.

The sphere was submerged in a viscous liquid inside a rectangular tank, made from 5 mm thick perspex sheets, with internal dimensions of width 125 mm, length 115 mm and height 200 mm. The sphere was carefully positioned at the centre of the tank such that the distance from the centre of the sphere to the side walls of the tank was approximately $8a$, while the flow field is predicted to decay with distance from the sphere according to an inverse cubic law, and so we estimate that the correction to the torque resulting from the boundaries is at most 0.2%. Experiments were performed in a temperature-controlled laboratory and the temperature inside the system was measured to be 19.89 ± 0.30 °C. The working fluid was silicone oil (Basildon Chemical Company Limited, UK) with a measured viscosity of $\nu = 924.14 \pm 5.29$ mm^2 s^{-1} and a measured density of $\rho_f = 975 \pm 1$ kg m^{-3}. The fluid-filled tank was positioned on a platform of adjustable height in the centre of Helmholtz coils of diameter 330 mm. The height and thickness of each Helmholtz coil was 140 mm and 35 mm respectively, and the gap between the two coils was 55 mm. The electromagnet inductance was 50 mH with a DC resistance of 0.36 ± 0.04 Ω. A spatially uniform, alternating magnetic field, $\mathbf{B} = B\mathbf{e}_z \sin(2\pi f t)$, where $\mathbf{e}_z$ is the unit vector in the vertical direction, was applied in order to study the angular response of the sphere from the zero-field position. Hall effect probes were used to measure the applied magnetic field, the amplitude B and frequency f of which varied from 0 to ~ 2.5 mT and from $0.01 - 2$ Hz, respectively.

Shielding from the Earth's magnetic field was achieved by placing the experimental system inside a Mumetal canister. Mumetal is a nickel-iron alloy with a magnetic permeability over 100 times greater than that of steel and shields by providing a path of low reluctance, and thus entraining magnetic flux. The Mumetal shield consisted of a 1.60 ± 0.02 mm thick cylindrical container, diameter and length of 510 mm and 520 mm respectively, with a lid and a base plate. Both the lid and base plate contained a centrally-located hole of 70 mm diameter through which cables could be passed to connect the experimental apparatus to control boxes and a PC, and permit observations of the motion of the spheres. The magnetic field inside the Mumetal shield was consistently found to be less than 5 μT, more than one order of magnitude smaller than the background field in the laboratory and also the geomagnetic field, which varies from 25 to 65 μT [24].

The sphere was illuminated using two 400 mm strips of 36 Light Emitting Diodes (LEDs). The strips were attached to the inside surfaces of the upper and lower coils of the electromagnet to illuminate the region of interest from above and below. This set-up produced uniform illumination across the observable surface of the sphere. Prior to each experiment, the axis of rotation of the sphere was carefully orientated orthogonal to the observational plane (as shown in the schematic diagram of the observed plane in Figure 1c) using a laser-sheet as a guide, such that $\phi = 0$ where ϕ is the angle between the magnetic-dipole axis of the sphere and the line-of-sight of the observer - the x-axis. The orientation of the sphere with respect to ϕ does not alter the dynamics, however, ensuring $\phi = 0$ was important for visualisation. The motion of the sphere was recorded using a Genie camera (HM-1400, Teledyne DALSA, Canada), with a spatial resolution of 1400×1024 pixels, which was positioned above the central hole of the lid of the Mumetal canister, as shown in Figure 1a. The light transmitted through the tank was directed to the camera in a periscope-like manner via three mirrors (M1, M2 and M3), of width 76 mm and height 102 mm, positioned in between the electromagnet and the Mumetal canister. Images of the sphere motion were typically acquired at a frame rate 100 times greater than the frequency of the applied field, except for frequencies > 0.6 Hz for which the images were acquired at the maximum frame rate of 64 Hz. The image resolution was 0.02 mm/pixel and the maximum recorded drift velocity of the sphere was ≈ 0.1 mm/min.

A schematic diagram of the experimental apparatus used for flow visualization is shown in Figure 2a. The velocity field was measured using Particle Image Velocimetry (PIV). Neutrally-buoyant, spherical microparticles (Fluostar particles, EBM Corporation, Japan) of 13.9 μm mean diameter were suspended in the viscous fluid and had a Rhodamine B coating which fluoresced under green-light laser illumination of wavelength 532 nm. A cross-section of the tank, corresponding to the rotational plane of the driven sphere, was illuminated from above and below using two green-light lasers and an arrangement of mirrors. A low-pass filter was positioned between the tank and the camera to reduce background noise in the detected signal. A high-speed camera (pco.1200 hs, PCO AG, Germany) with a spatial resolution of 1280×1024 pixels was used to image the region of interest. The camera was positioned orthogonal to the illuminated plane, synchronised with the Nd:YAG pulsed laser using a pulse generator (BNC Model 500, Oxford Lasers Ltd., UK) and imaged at a

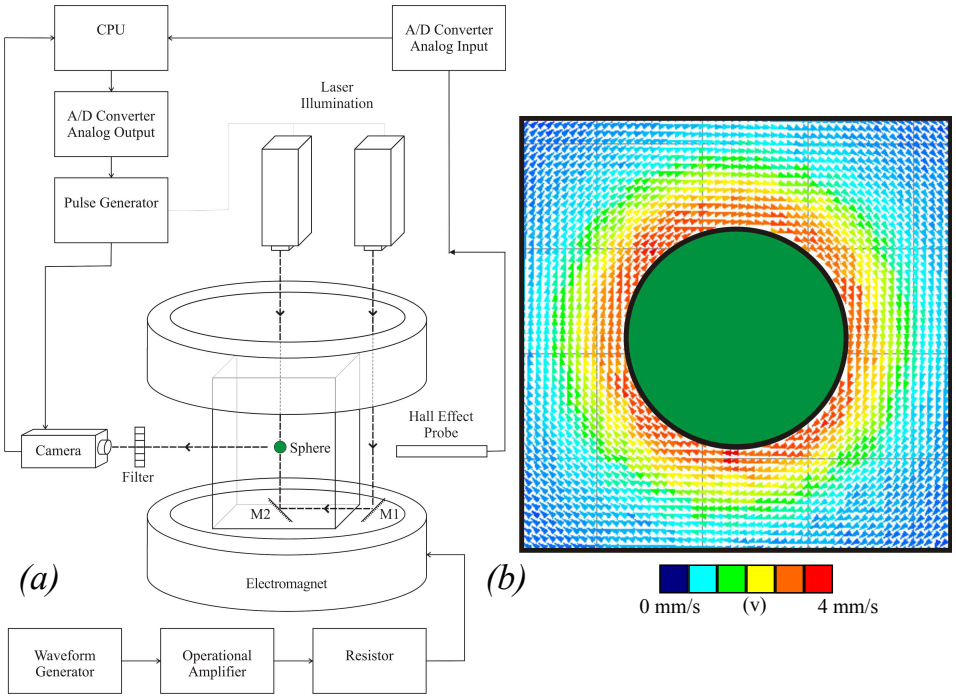

Fig. 2: [Colour online] (a) Schematic diagram of the experimental apparatus used for flow visualisation. Illumination of the rotational plane of the sphere was provided by lasers and an optical arrangements of mirrors (M1 and M2). A high-speed camera was positioned orthogonal to the illuminated plane and a low-pass filter was positioned between the tank and the camera to remove noise from the signal. (b) A typical velocity vector field depicting the flow generated by a spherical particle rotating, in the clockwise direction, in a viscous fluid. The instantaneous velocity field was measured using Particle Image Velocimetry at $3\pi/10$ in the oscillation cycle. The green circle in the centre of the image denotes the sphere. The vectors are represented by coloured arrows, the magnitude of which ranges from 0 $\mathrm{mm\,s^{-1}}$ (dark blue) to 4 $\mathrm{mm\,s^{-1}}$ (dark red).

rate of 15 Hz, the maximum pulse-rate of the Nd:YAG laser, with an exposure of between 10 and 20 ms. Pairs of consecutive images were then subject to sub-pixel PIV. A consequence of the maximum pulse rate of the laser was that flow visualisation measurements were conducted for a frequency of applied magnetic field of 0.15 Hz. For flow visualization, the Mumetal canister was removed from the apparatus, this was found not to have a significant effect on the response of the sphere to applied forcing [3].

A typical, instantaneous velocity vector field, obtained at $3\pi/10$ in the oscillation cycle of the sphere, is shown in Figure 2b. The sphere was rotating in the clockwise direction which induced rotation of the surrounding fluid in the same direction. The velocity vectors are represented by arrows, the colour of which denotes the magnitude of the velocity which ranges from 0 $\mathrm{mm\,s^{-1}}$ to 4 $\mathrm{mm\,s^{-1}}$. The velocity vector field shows that the velocity of the fluid is greatest close to the surface of the sphere and decreases with radial distance from the sphere surface.

3 Theory

3.1 Modelling the motion of the sphere

The dynamic response of a sphere, containing a magnetic dipole, to an applied magnetic field and subject to hydrodynamic and gravitational forces is considered theoretically in this section. A schematic of the coordinate system used in the development of the model is shown in Figure 1b. We define θ as the instantaneous angle between the magnetic dipole orientation and the horizontal x-y plane, and θ_0 as the value of θ when the sphere is at rest in the absence of applied magnetic field. The distribution of weights inside in the sphere was chosen to minimize θ_0 such that the orientation of the magnetic dipole of the sphere with zero applied field was approximately horizontal in the eyes of the observer.

Under the assumptions that $Re = 0$ and that the sphere is rotating in unbounded fluid, the equation of motion for the dynamic response of a sphere subject to an applied magnetic field can be deduced from a

combination of the viscous, gravitational and magnetic torques acting about the centre of the sphere:

$$8\pi\mu a^3\frac{d\theta}{dt} = -\epsilon\sin(\theta-\theta_0) + Bm\sin\omega t\cos\theta, \quad (1)$$

where μ is the dynamic viscosity of the fluid, a is the radius of the sphere, ω is the angular frequency, ϵ is the magnitude of the gravitational torque which acts to return the sphere towards the zero applied field orientation at $\theta=\theta_0$, B is the magnetic field strength and m is the magnetic moment of the magnetic-dipole of the sphere. For a rigid distribution inside the sphere ϵ is equal to $Mg\lambda a$, where $M = 4\pi a^3\rho_s/3$ and λa is the distance that the centre of mass of the sphere is displaced from the centre of the sphere. The viscous torque arises due to hydrodynamic resistance to the motion of the sphere. The gravitational torque arises from gravity acting on the non-uniform mass distribution within the sphere and acts to return the magnetic-dipole of the sphere to the zero-field position. The magnetic torque results from the interaction of the magnetic dipole of the sphere and the applied field and acts to align the magnetic-dipole of the sphere with the applied field. We note that the ball is so close to spherical that the centre of mass of the displaced fluid can be taken as the centre of sphere, and so there is no buoyancy contribution to the torque balance (1).

A non-dimensional time, based on the angular frequency ω of the applied oscillatory field, can be defined as $\hat{t}=\omega t$. Equation 1 then becomes

$$\frac{d\theta}{d\hat{t}} = -\frac{\epsilon}{8\pi\mu a^3\omega}\sin(\theta-\theta_0) + \frac{Bm}{8\pi\mu a^3\omega}\sin\hat{t}\cos\theta. \quad (2)$$

Dimensionless parameters which quantify the ratio of the gravitational torque to the viscous torque, ϵ, and the viscous torque to the magnetic torque, Ma, acting on the sphere are thus defined by:

$$\hat{\epsilon} = \frac{1}{\omega T_0}, \quad \frac{1}{Ma} = \frac{Bm}{8\pi\mu a^3\omega}, \quad (3)$$

respectively, where $T_0 = 8\pi\mu a^3/\epsilon$ is the gravitational time-scale, discussed in further detail in §3.2, and Ma is the Mason number [22]. This Ordinary Differential Equation (ODE) for θ can thus be written as

$$\frac{d\theta}{d\hat{t}} = -\hat{\epsilon}\sin(\theta-\theta_0) + \frac{1}{Ma}\sin\hat{t}\cos\theta. \quad (4)$$

As the amplitude of oscillation, θ_1, may be as large as 90° degrees, we solve equation 4 numerically by direct integration; this requires a single initial condition, for example the value of θ when $\hat{t}=0$. In the case $\hat{\epsilon}=0$ (where the sphere is perfectly balanced and so has no preferred resting orientation), we can separate equation 4 and integrate to find $\theta(\hat{t})$ analytically. All solutions for $\theta(\hat{t})$ are periodic with period 2π, and form a two parameter family characterised by the mean value of θ, denoted by $\bar{\theta}$, and the Mason number Ma. The solution for the equations with $\hat{\epsilon}=0$ and $\bar{\theta}=0$ satisfies $\theta_{min} = -\theta_{max}$ and

$$Ma^{-1} = \ln(\sec(\Delta\theta/2) + \tan(\Delta\theta/2)), \quad (5)$$

where $\Delta\theta$ is the change in θ over a period of oscillation.

When $\hat{\epsilon} > 0$, the solution $\theta(\hat{t})$ takes several cycles to converge towards a periodic solution. We can determine the periodic limit cycles numerically by solving a boundary value problem in Matlab (R2011a, Mathworks, USA) with periodic boundary conditions, using the in-built function *bvp5c*. We find that the resulting limit cycles have mean close to zero, but do not satisfy generally equation 5. However, in the limit of very small $\hat{\epsilon}$ we retain the condition that $\bar{\theta}=0$, and the amplitude of the limit cycles satisfies (5).

3.2 Gravitational Time-scale

Individual spheres have unique, non-uniform mass distributions, an inevitable result of the embedding of magnets and weights. This non-uniform mass distribution supplies a net gravitational torque ϵ which acts to return the sphere towards a preferred orientation $\theta=\theta_0$. The embedded weights were positioned so that θ_0 is close to zero, and hence the magnetic dipole is close to horizontal when zero magnetic field is applied.

In order to characterise the dynamic response of a sphere to the applied field, a precise measure of the gravitational torque was required. A simple test involved measuring the rate at which the sphere returns to the zero-field position when released from a non-zero angle in the absence of magnetic forcing. With $B=0$, equation 1 becomes

$$\frac{d\theta}{dt} = -\frac{\epsilon}{8\pi\mu a^3}\sin(\theta-\theta_0). \quad (6)$$

For small displacements, $\sin(\theta-\theta_0)\approx\theta-\theta_0$, and so $\theta-\theta_0 \propto \exp(-t/T_0)$, with time constant

$$T_0 = \frac{8\pi\mu a^3}{\epsilon}. \quad (7)$$

Estimates of the time-scale associated with the gravitational torque were obtained by measuring the decay of the angular position of a sphere from an offset position towards the zero-field state upon sudden removal of the applied magnetic field. A large ($\sim$ 2.2 mT) steady

magnetic field was applied initially in order to attain alignment of the magnetic dipole with the applied field. Sudden removal of the applied field led to the rotation of the sphere back to the zero-field position under the influence of gravity. A time-series of the angular position of the sphere was obtained from an initial angle of 30° to the zero-field orientation, as shown in Figure 3a. A least-squares fit of the form $\theta = a\exp(-t/T) + b$ yielded $a = 28.21°$, $b = 3.22°$ and $T = 4.67$ s. The initial angle of 30° is sufficiently small that numerical solutions of (6) are almost indistinguishable from $\theta = a\exp(-t/T) + b$, and so the small angle approximations used to derive exponential decay are valid.

The importance of the gravitational torque in our model is expressed through the dimensionless parameter $\hat{\epsilon} = 1/(\omega T_0)$. In our experiments, the frequency of the magnetic field ranged from 0.01 to 2 Hz, yielding $\hat{\epsilon}$ in the range 0.017 to 3.5. Thus gravitational torque is typically not negligible in our experiments.

This measurement of T_0 not only allows us to calculate $\hat{\epsilon}$ but also supplies information regarding the mass distribution within the ball. We note that

$$\epsilon = \frac{8\pi\mu a^3}{T_0} = \frac{4\pi a^4 \rho_s g \lambda}{3} \tag{8}$$

where λa is the displacement of the centre of mass of the sphere. With $T_0 = 4.67$ s, we find that $\lambda = 0.015$, implying a slight offset of the centre of mass from the centre of the sphere. Any non-sphericity of the ball could lead to an offset of the centre of mass fluid displaced by the ball from the centre of the ball, and thus lead to a small buoyancy torque. This term would appear in the torque balance in same form as the gravitational torque due to the displacement of centre of mass of the weighted ball, and so can be absorbed into T_0 in our model.

4 Results

4.1 Magnetic actuation and response of the sphere

For small angular displacement, an approximate solution to equation 4 is given by $\theta = \theta_0 + \theta_1 \sin(\omega t + \varphi)$, where θ_1 is the amplitude of oscillation and $\varphi = -\arctan(2\pi T_0 f) = \arctan(\hat{\epsilon}) - \pi/2$ is the phase difference between the applied magnetic field and the response of the sphere. The phase difference, φ is negative as the oscillatory motion of the sphere lags the applied magnetic field. Experimentally measured values of φ are shown as a function of frequency of applied field, f in Figure 3b for a magnetic field strength of $B = 1.654 \pm 0.005$ mT. The measured phase delay increases from $< \pi/10$ at a frequency of 0.025 Hz and saturates at $\approx \pi/2$ for frequencies above 0.25 Hz. Typically, measurement of the dynamic response of the sphere to the applied field were obtained at a frequency of 0.5 Hz for which the phase delay was $\approx \pi/2$.

The analytic solution, $\varphi = -\arctan(2\pi T_0 f)$, for the phase delay for small-amplitude oscillations and numerical solutions for large-amplitude oscillations are also included in Figure 3b. Both the small amplitude solution and the full numerical solution for the phase delay show the same qualitative behaviour as the experimental results, with $\varphi = 0$ at very low frequencies, and φ decreasing monotonically towards $-\pi/2$ as f increases. However, the full numerical solutions are in much better quantitative agreement with the experimental results. The effect of the amplitude and frequency of the applied field on the angular displacement of the sphere is discussed in greater detail later in this section, in terms of Ma and $\hat{\epsilon}$, yet here we see the influence of the frequency of applied field on the dynamic response of the sphere. For constant $B = 1.654 \pm 0.005$ mT, the amplitude of oscillation (also included in Figure 3b) increased with decreasing f such that for $f = 1$ Hz, $\theta_1 \approx 16°$, while for $f \leq 0.1$ Hz, $\theta_1 \approx 90°$. For this reason we find that the numerical findings for large-amplitude oscillations agree better with the experimental results than the analytic solution at small f.

Experimental time-series of the angle of the sphere, $\theta(t)$, are shown in Figure 3c, for $\hat{\epsilon} = 0.22$ and $Ma = 4.85$, 2.43, 1.21, 0.48 and 0.20 (top-to-bottom), which corresponds to applied magnetic fields of amplitude 0.112 ± 0.015, 0.224 ± 0.015, 0.448 ± 0.015, 1.122 ± 0.015 and 2.688 ± 0.015 mT, respectively. In each case, four periods of oscillation are shown and the series have been shifted in time such that $\theta = 0$ at $t = 0$.

4.2 Dependence of the sphere response on Ma

When Ma is large, $Ma \gg 1$, the induced magnetic torque is small compared with the viscous resistance to motion, and so the sphere performs small-amplitude torsional oscillations about the zero-field orientation. The oscillations are sinusoidal and match the waveform of the applied field such that the response of the sphere is proportional to the magnetic forcing. For decreasing Ma, the amplitude of oscillation increases nonlinearly. Furthermore, the response of the sphere deviates increasingly from the sinusoidal form of the applied field as alignment of the magnetic axis with the applied field in both direction is approached. A sinusoidal function was fitted to the experimental data using a least-squares method and, for oscillations of amplitude less than 19°, the standard deviation between the fitted function and the experimental data was less than 0.1%. Moreover, for oscillations of amplitude less than 45°, which resulted

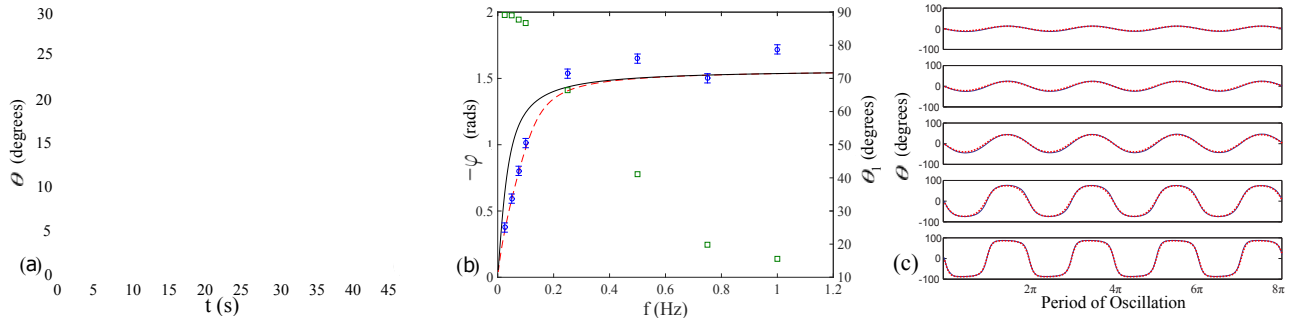

Fig. 3: [Colour online] (a) A time-series of the angular position of the magnetic-dipole axis of the sphere measured as a function of time as the sphere rotates back to the zero-field orientation under the sole influence of gravity. A least-squares fit of the data to $\theta = a\exp(-t/T) + b$ yielded $a = 28.21°$, $b = 3.22°$ and $T_0 = 4.67$ s. (b) The phase delay, φ, between the applied magnetic field and the resulting motion of the sphere given by $\varphi = -\arctan(2\pi T_0 f)$ for small-amplitude oscillations (solid line), calculated numerically for large-amplitudes (dashed line) and measured experimentally (○) as a function of the frequency of applied field, for $B = 1.654 \pm 0.005$ mT. The experimental amplitude of angular oscillation θ_1 is also shown (□) as a function of frequency (with scale on the right-hand axis). (c) Experimental (solid line) and numerical (dots) time-series of the angular displacement of the driven, magnetic sphere over four periods of oscillation, for $\hat{\epsilon} = 0.22$ and $Ma = 4.85$, 2.43, 1.21, 0.48 and 0.20 (top-to-bottom). The response of the sphere deviates increasingly from the form of the sinusoidal drive with decreasing Ma.

for $Ma \approx 1.2$, the standard deviation between the data and the fitted sinusoidal function was less than 1%.

For small Mason number, $Ma \ll 1$, the ratio of the magnetic torque to viscous torque acting on the sphere is large, resulting in large-amplitude oscillations which deviate significantly from the sinusoidal form of the applied field. The magnetic dipole quickly attains approximate alignment with the applied field, saturating the angular response at $\pm 90°$, and remaining in that position until the field reverses direction. For the larger values of Ma shown in Figure 3c, the form of the sphere response is symmetric under time reversal. However, for $Ma = 0.20$, the measured $\theta(t)$ is noticeably asymmetric with respect to time. The origin of the asymmetry is the gravitational torque, which always acts to return the sphere towards $\theta = \theta_0$, and can act with or against the driving magnetic torque at different points in the cycle. The dimensionless parameter $\hat{\epsilon}$ quantifies the size of the gravitational torque relative to viscous torque, and so we expect symmetric behaviour for $\hat{\epsilon} = 0$ and highly asymmetric behaviour at large $\hat{\epsilon}$.

4.3 Angular displacement of the sphere

The total angular displacement of the sphere throughout the oscillation cycle is zero. The maximum angular displacement of the sphere $\Delta\theta = 2\theta_1$, equal to the change in θ over a period of oscillation, was investigated as a function of both the magnetic torque Ma, and the gravitational torque $\hat{\epsilon}$, and is shown as a function of Ma for various $\hat{\epsilon}$ in Figure 4a. The experimental data are shown in Figure 4a alongside numerical results obtained for parameters corresponding to the experiments. The analytic solution to the governing equations of motion obtained for $\hat{\epsilon} = 0$ (see Equation 5) is also included on the figure, as are further numerical results determined as a function of Ma for $\hat{\epsilon} = 0.44$, $\hat{\epsilon} = 0.67$, $\hat{\epsilon} = 1.33$ and $\hat{\epsilon} = 3.34$. Good agreement is found between the experimental and numerical findings when using the same values of Ma and $\hat{\epsilon}$. Furthermore, the experimental data points with small values of $\hat{\epsilon}$ lie close to the analytical prediction from equation 5, which is the analytical solution in the limit $\hat{\epsilon} = 0$.

When Ma is held constant, the maximum angular displacement of the sphere, $\Delta\theta$, is significantly reduced for $\hat{\epsilon} \gg 1$ because the gravitational torque acts more strongly to return the sphere to the zero-field position. For $Ma \ll 1$, $\Delta\theta$ typically is close to 180°, and moves closer to this maximum value when $\hat{\epsilon}$ is decreased. We can calculate the characteristic value of $\hat{\epsilon}$ which prevents the angular displacement reaching the maximum value. We initially compute the required Ma which ensured $\Delta\theta$ was within 1% of the maximum response of 180° when $\hat{\epsilon} = 0$, this was found to be $Ma = 0.21$. We consider the effect of $\hat{\epsilon}$ to be significant when it reduces $\Delta\theta$ by 5%. For $Ma = 0.21$, this was found to occur at $\hat{\epsilon} = 0.396$ through numerical investigation. The maximum angular displacement of the sphere, $\Delta\theta$, measured as a function of Ma for $\hat{\epsilon} < 0.396$ is shown in figure 4b. The deviation of the angular displacement of the sphere from that predicted by the analytical solution is small and only apparent at angular displacements of

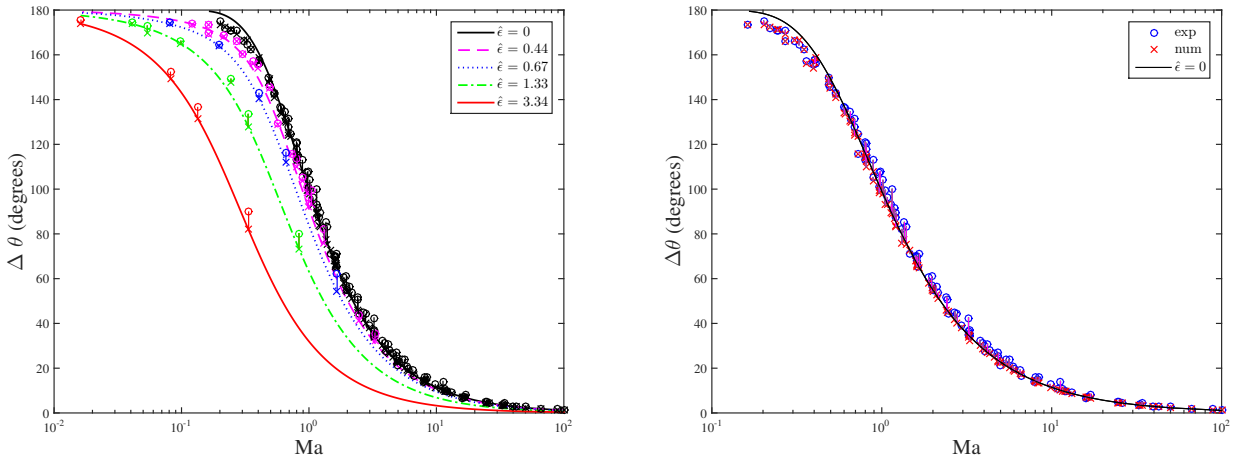

(a) (b)

Fig. 4: [Colour online] (a) The maximum angular displacement of the sphere, $\Delta\theta$, measured as a function of the dimensionless parameter Ma for various $\hat{\epsilon}$. Experimental data (○) and numerical data (×) evaluated at the corresponding parameters are connected by a vertical line. The colour scheme for data points is: $\hat{\epsilon} < 0.22$ (black), $0.22 < \hat{\epsilon} < 0.56$ (magenta), $0.56 < \hat{\epsilon} < 1$ (blue), $1 < \hat{\epsilon} < 2.34$ (green), $2.34 < \hat{\epsilon}$ (red). The error bars on the experimental data points would be smaller than the data markers, and for clarity are not shown here. The analytical solution for the case when the gravitational torque acting on the sphere is zero, $\hat{\epsilon} = 0$, is represented by the solid, black line. Numerical results determined as a function of Ma for $\hat{\epsilon} = 0.44$, $\hat{\epsilon} = 0.67$, $\hat{\epsilon} = 1.33$ and $\hat{\epsilon} = 3.34$ are depicted by connecting numerical data points, and are represented as indicated in the legend. (b) $\Delta\theta$ measured as a function of Ma for $\hat{\epsilon} < 0.396$. Experimental data (○) and numerical data (×) evaluated at the corresponding parameters are connected by a vertical, magenta line. The analytical solution for $\hat{\epsilon} = 0$ is represented by the solid, black line.

close to 180°, for which gravitational torque prevents the sphere from attaining alignment with the applied field in both directions. For $\hat{\epsilon} > 0.396$, however, the maximum angular displacement which the sphere can attain is significantly reduced compared to the $\hat{\epsilon} = 0$ results. The experimental and numerical data obtained for $\hat{\epsilon} > 0.396$ shown in Figure 4a clearly differ from the analytical solution for $\hat{\epsilon} = 0$.

4.4 Flow Field

Quantitative measurements of the flow were obtained, using the PIV technique outlined in §2, for a sphere performing small-amplitude torsional oscillations of a sinusoidal form as a result of an applied magnetic field of 0.15 Hz. The penetration depth of the flow, $\delta \sim (\frac{\nu}{\omega})^{1/2} = 31.3$ mm, was large compared to the radius of the sphere, $\delta \gg a$, which implies that $a^2\omega \ll \nu$. Considering that $\alpha^2 = a^2\omega/\nu = 0.064 \ll 1$ and that $Re = av_{max}/\nu \approx 0.03$, we conclude that the motion of the sphere occurred in the low-frequency, low-Re limit [17].

In the case of low Re and low frequencies of oscillation, the fluid velocity varies only slowly with time, so that the flow can be regarded as steady at any given instant, and the time-scale associated with the angular acceleration is significantly larger than the viscous time-scale (a^2/ν) such that the contribution of the acceleration torque to the viscous torque is negligible compared to that of the quasi-steady torque [8, 19]. The fluid velocity resulting from the torsionally oscillating sphere can therefore be reasonably compared with the analytical solution of the fluid velocity generated in the equatorial plane by the steady rotation of a sphere in an unbounded, incompressible viscous fluid [14]:

$$v = \frac{\Omega a^3}{r^2} \tag{9}$$

where Ω is the angular velocity of the sphere, a is the sphere radius, r is the radial distance from the centre of the sphere.

The magnitude of the fluid velocity was calculated from the experimental vector fields, a typical example of which is shown in Figure 2b. The observed symmetry of the flow about the axis of rotation of the sphere enabled spatial averaging around 360° of the vector

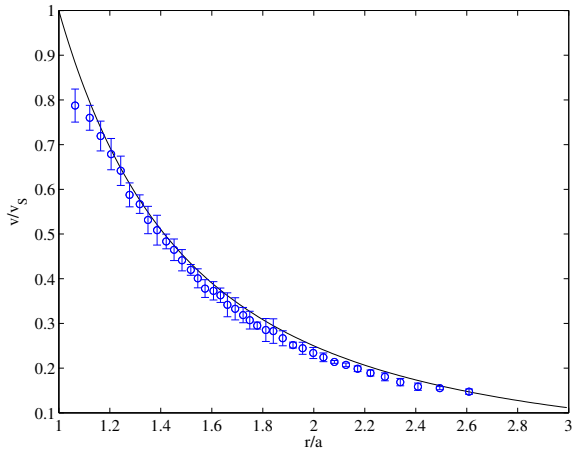

Fig. 5: The instantaneous fluid velocity measured as a function of radial distance. The fluid velocity v has been normalised by the surface velocity of the sphere v_S, and the radial distance r has been normalised by the radius of the sphere a. The black curve is the analytical solution for the fluid velocity resulting from a sphere rotating with constant angular velocity in an infinite fluid [14]. The blue data points (○) represent the experimental velocity, the standard deviation of which is given by the error bars. Measurements were made for $Ma = 2.01$ and $\hat{\epsilon} = 0.22$ for which the sphere performed torsional oscillations of amplitude $\theta = 28°$ that approximated a sinusoidal function to within 1%.

field. The measured fluid velocity resulting from the small-amplitude, low-frequency torsional oscillations of a sphere and the fluid velocity calculated from the analytical solution for a sphere undergoing steady rotation, given by equation 9, are both shown in Figure 5. The experimental data points shown in Figure 5, obtained at $3\pi/10$ in the oscillation cycle, are typical of instantaneous measurements obtained throughout the period of oscillation.

Good quantitative agreement is found between the experimental and analytical fluid velocity as a function of radial distance. This agreement validates the model described in §3 which, in deriving the viscous torque acting on the sphere, assumed that $Re = 0$ such that the velocity field is given by equation 9. The significant deviation of the experimental data from the analytic solution close to the sphere results from specular reflections by the surface of the sphere which, prior to diffusing, illuminate tracer particles that are not on the equatorial plane. The marginal reduction in agreement at a radial distance $\gtrsim 2$ is attributed to the influence of the boundaries of the tank containing the viscous fluid which were $\approxeq 8a$ from the centre of the sphere.

5 Concluding remarks

A near neutrally buoyant sphere with a magnetic-dipole axis and a non-uniform mass distribution was submerged in a viscous fluid and subjected to an periodically-oscillating magnetic field. For low frequency oscillations ($a^2\omega \ll \nu$) of small amplitude at low-Reynolds number ($v_{max}a/\nu \ll 1$), such that the flow can be regarded as steady at any given instant [17], good agreement was found between experimental measurements of the fluid velocity around the sphere and the analytical solution of the functional dependence of the fluid velocity on radial distance from a sphere performing steady rotational oscillations in an infinite, viscous fluid. This confirms that the set up is an experimental realisation of a Stokes flow in which the oscillatory motion of particles can be actuated via a non-contact method, removing from the flow field the uncharacterised effects which are introduced by the motion of a supporting rod or torsion fibre. Having developed an experimental technique that enables the remote control of the torsional oscillations of a free sphere in a fluid at low-Re, it would be instructive to conduct an investigation of the flow field for $Re \gg 1$ and compare the results to the work of Hollerbach *et al.* [12] in order to determine what effect the connecting rod has on the development of the secondary circulatory flow.

The developed experimental apparatus provides a controlled environment in which other low-Re phenomena may be explored, such as the influence of nearby boundaries on the motion of a torsionally oscillating sphere and the hydrodynamic interaction between a magnetically-controlled *active* sphere with a characterised driving force and non-magnetic *passive* spheres. The interaction between configurations of multiple *active* and *passive* spheres could potentially be used to develop magnetically-actuated mixing devices and micro-fluidic pumps and is the subject of our current investigation.

The set up also permits examination of the effect of tethers on the motion of oscillating spheres. It would of interest to study the fluid-structure interaction of an actuated sphere connected to an elastic tether, as a simple low-Re swimmer may result. The torsional oscillations of the swimmer body would actuate the elastic tail, generating a bending wave that propagates along the elastic filament and propels the sphere through the fluid [18]. Previously, synthetic swimmers of a similar design have developed by Wiggins *et al.* [25] and Yu *et al.* [26], and numerical studies [21] showed that a magnetic dipole with a flexible tail behaves as a swimmer when subject to AC magnetic fields.

Acknowledgements The authors would like to acknowledge the technical assistance of P. Tipler and to thank Professor Sir K. Novoselov FRS and Professor A. Murray for the loan of equipment. The completion of the experimental work was supported by an EPSRC studentship (EP/P505631/1), and the writing of the manuscript by a David Crighton Fellowship.

References

1. Ambari, A., Gauthier-Manuel, B., Guyon, E.: Wall effects on a sphere translating at constant velocity. J. Fluid Mech. **149**, 235–253 (1984)
2. Benson, C.B., Hollis Hallett, A.C.: The oscillating sphere at large amplitudes in liquid helium. Can. J. Phys. **34**, 668–678 (1956)
3. Box, F.: An experimental investigation of oscillating spheres in a very viscous fluid. Ph.D. thesis, University of Manchester, UK (2014)
4. Buchanan, J.: The oscillations of a spheroid in a viscous liquid. Proc. Lond. Math. Soc. **22**, 181–214 (1891)
5. Carrier, G.F., Di Prima, R.C.: On the torsional oscillations of a solid sphere in a viscous fluid. J. Appl. Mech. **23**, 601–605 (1956)
6. Chen, S.: The resistive force on a sphere with a string moving in a viscous fluid. Chin. J. Phys. **32(4)**, 395–404 (1994)
7. Di Prima, R.C., Liron, N.: Effect of secondary flow on the decaying torsional oscillations of a sphere and a plane. Phys. Fluids **19**, 1450 (1976)
8. Feuillebois, F., Lasek, A.: On the rotational historic term in non-stationary Stokes flow. Q. J. Mech. Appl. Math. **31(4)**, 435–443 (1978)
9. Folse, R.F.: Observations of secondary flows generated by a torsionally oscillating sphere in linearly stratified fluids. Phys. Fluids **6**, 537 (1994)
10. Folse, R.F., Strahan, A.E., Nail, J.M.: High-amplitude torsional oscillations of a sphere in a viscous fluid. Phys. Fluids **17**, 1774 (1974)
11. Helmholtz, H.v., Piotrowski, G.v.: Über Reibung tropfbarer Flüssigkeiten. S.B. Akad. Wiss. Wein. **40**, 607–658 (1860)
12. Hollerbach, R., Weiner, R.J., Sullivan, I.S., Donnelly, R.J., Barenghi, C.F.: The flow around a torsionally oscillating sphere. Phys. Fluids **14**, 4192 (2002)
13. Jackson, J. D.: Classical Electrodynamics Third Edition, 3rd edn. Wiley (1998)
14. Jeffery, G. B.: On the steady rotation of a solid of revolution in a viscous fluid. Proc. Lon. Math. Soc. **14**, 327,338 (1915)
15. Kestin, J., Persen, L.N.: Small oscillations of bodies of revolution in a viscous fluid. Brown University Report AF-891/2, Contract A718(600)-891 (1954)
16. Lamb, H.: Hydrodynamics, 6th edn. Dover (1932)
17. Landau, L. D. and Lifshitz, E. M.: Fluid Mechanics, 2nd edn. Butterworth-Heineman (1987)
18. Lauga, E.: Floppy swimming: viscous locomotion of actuated elastica. Phys. Rev. E **75**, 041,916 (2007)
19. Lei, U., Yang, C.Y., Wu, K.C.: Viscous torque on a sphere under arbitrary rotation. Appl. Phys. Lett. **181908**, 1–24 (2006)
20. Lim, E.A., Kobayashi, M.H., Coimbra, C.F.M.: Fractional dynamics of tethered particles in oscillatory Stokes flows. J. Fluid Mech. **746**, 606–625 (2014)
21. Livanovičs, R., Cēbers, A.: Magnetic dipole with a flexible tail as a self-propelling microdevice. Phys. Rev. E **85**, 041,502 (2012)
22. Man, Y., Lauga, E.: The wobbling-to-swimming transition of rotated helices. Phys. Fluids **25**, 071,904 (2013)
23. Mondy, L.A., Grillet, A.M., Pacheco, G., Henfling, J., Ingber, M.S., Graham, A.L., Brenner, H.: Apparent slip at the surface of a ball spinning in a concentrated suspension. J. Fluid Mech. **538**, 377–397 (2005)
24. NOAA/NGDC and CIRES: US/UK World Magnetic Model – Epoch 2010.0 Main Field Total Intensity (F) (2010). URL `http://www.ngdc.noaa.gov/geomag/WMM/data/WMM2010/WMM2010_F_MERC.pdf`
25. Wiggins, C.H., Riveline, D., Ott, A., Goldstein, R.E.: Trapping and wiggling: elastohydrodynamics of driven microfilaments. Biophys. J. **74(2)**, 1043–1060 (1998)
26. Yu, T.S., Lauga, E., Hosoi, A.E.: Experimental investigations of elastic tail propulsion at low Reynolds number. Phys. Fluids **18**, 091,701 (2006)
27. Yunsheng High-Tech Magnetics Co. Ltd.: Brochure and Product Catalogue (2008)